Nuclear moments and isotope shifts of the actinide isotopes $^{249–253}$Cf probed by laser spectroscopy

Felix Weber,[1,*] Thomas E. Albrecht-Schönzart,[2] Saleh O. Allehabi,[3] Sebastian Berndt,[1,4] Michael Block,[4,5,6] Holger Dorrer,[4] Christoph E. Düllmann,[4,5,6] Vladimir A. Dzuba,[3] Julie G. Ezold,[7] Victor V. Flambaum,[3] Vadim Gadelshin,[1] Stephane Goriely,[8] Ashley Harvey,[7] Reinhard Heinke,[9] Stephane Hilaire,[10,11] Magdalena Kaja,[1] Tom Kieck,[5,6] Nina Kneip,[1] Ulli Köster,[12] Jeremy Lantis,[5,6] Christoph Mokry,[4,6] Danny Münzberg,[5,6] Steven Nothhelfer,[5,6] Stephan Oberstedt,[13] Sophie Péru,[10,11] Sebastian Raeder,[5,6] Jörg Runke,[4,5] Volker Sonnenschein,[14] Matou Stemmler,[1] Dominik Studer,[1] Petra Thörle-Pospiech,[4,6] Hideki Tomita,[14] Norbert Trautmann,[4] Shelley Van Cleve,[7] Jessica Warbinek,[4,5] and Klaus Wendt[1]

[1]*Institut für Physik, Johannes Gutenberg-Universität Mainz, 55099 Mainz, Germany*
[2]*Florida State University, Tallahassee, Florida 32300-32399, USA*
[3]*School of Physics, University of New South Wales, 2052 Sydney, Australia*
[4]*Department Chemie–Standort TRIGA, Johannes Gutenberg-Universität Mainz, 55099 Mainz, Germany*
[5]*GSI Helmholtzzentrum für Schwerionenforschung GmbH, 64291 Darmstadt, Germany*
[6]*Helmholtz-Institut Mainz, 55099 Mainz, Germany*
[7]*Oak Ridge National Laboratory, Oak Ridge, Tennessee 37831, USA*
[8]*Institut d'Astronomie et d'Astrophysique, CP-226, Université Libre de Bruxelles, 1050 Brussels, Belgium*
[9]*CERN, 1211 Geneva, Switzerland*
[10]*CEA, DAM, DIF, F-91297 Arpajon, France*
[11]*Laboratoire Matière en Conditions Extrêmes, CEA, Université Paris-Saclay, 91680 Bruyères-le-Châtel, France*
[12]*Institut Laue Langevin, 38042 Grenoble, France*
[13]*European Comission, Joint Reserach Centre (JRC), 2440 Geel, Belgium*
[14]*Department of Energy Engineering, Nagoya University, 464-8603 Nagoya, Japan*

(Received 20 December 2022; accepted 7 February 2023; published 21 March 2023)

We report on high-resolution laser spectroscopy studies on $^{249–253}$Cf with spectral linewidths in the order of 100 MHz carried out at the RISIKO mass separator at Mainz University. In total three atomic ground-state transitions were investigated and the hyperfine parameters for the odd-A isotopes and isotope shift for all examined isotopes have been determined from the measured spectra. The isotope shift measurements allowed tracking of changes in mean-squared charge radii across the deformed nuclear shell closure at $N = 152$, whereby shape discontinuities were not observed. Experimental hyperfine coupling constants of the atomic ground state were combined with relativistic many-body atomic calculations to extract the nuclear magnetic-dipole moment of ^{249}Cf with improved precision to $\mu_I(^{249}\mathrm{Cf}) = -0.395(17)\mu_N$, whereas $\mu_I(^{251}\mathrm{Cf}) = -0.571(24)\mu_N$ and $\mu_I(^{253}\mathrm{Cf}) = -0.731(35)\mu_N$ were derived for the first time. Additionally, the spectroscopic quadrupole moments $Q_S(^{249}\mathrm{Cf}) = 6.27(33)$ eb and $Q_S(^{253}\mathrm{Cf}) = 5.53(51)$ eb were extracted.

DOI: 10.1103/PhysRevC.107.034313

I. INTRODUCTION

High-resolution laser spectroscopy is a versatile technique to study nuclear ground-state properties such as spins, electromagnetic moments, and changes of mean-squared charge radii along isotopic chains [1,2]. These have been precisely measured in recent years, also on exotic short-lived isotopes produced at several radioactive ion-beam (RIB) facilities. Heavy actinides are of specific interest as they exhibit stabilizing nuclear shell effects, which are of particular relevance for theoretical predictions of superheavy elements [3]. Of particular interest are the changes of mean-squared charge radii across the deformed nuclear shell closure at neutron number $N = 152$ [4,5], which allow exploring of variations in the nuclear shape in this region. Previous measurements revealed the increase of the nuclear charge radius with neutron number to be significantly enhanced beyond the neutron shell closures at $N = 82$ and $N = 126$ [6], which is referred to as a kink. However, the very limited and incomplete information on atomic levels specifically for actinides beyond plutonium hamper high-resolution spectroscopy on atomic transitions [7,8]. A number of longer-lived isotopes of actinide elements up to fermium (atomic number $Z = 100$) can be produced by multiple neutron captures and decays

*wfelix02@uni-mainz.de

in a high flux reactor, such as the high-flux isotope reactor (HFIR) at the Oak Ridge National Laboratory (ORNL) [9]. In this way, several isotopes of these elements have become accessible for studies at off-line ion-beam facilities, i.e., at experimental setups that are separated from the production site. Studies on such samples require the chemical isolation of the element of interest from the irradiated target. Using such off-line samples, the atomic level structures of californium ($Z = 98$) [10] and einsteinium ($Z = 99$) [11] have been comprehensively investigated at the RISIKO mass separator at Johannes Gutenberg University Mainz (JGU), and efficient ionization schemes, including autoionizing states, have been identified. Furthermore, the hyperfine structures (HFSs) of different einsteinium isotopes were measured, which enabled the extraction of nuclear moments [12]. For californium, however, the HFS splitting is much less pronounced than for einsteinium due to the lower nuclear magnetic moment, which is a consequence of proton pairing in even-Z nuclei. The magnetic moment of ^{249}Cf is reported to $\mu_I = -0.28(6)\mu_N$, with the absolute value stemming from an electron parametric resonance spectrum in conjuction with atomic calculations [13], and the sign stemming from optically observed hyperfine splittings in electrodeless lamp spectra [14]. It is the only reported magnetic moment for californium; electric-quadrupole moments are yet unknown. Nuclear spins of $I = 9/2^-$ and $I = 1/2^+$ were firmly assigned to the isotopes ^{249}Cf and ^{251}Cf, respectively, derived from nuclear decay systematics [15,16]. A nuclear spin of $I = 7/2^+$ was tentatively allocated to the ground state of ^{253}Cf according to the assignment to a 7/2[613] Nilsson-model state, although its nuclear decay is also compatible with a spin of 9/2 [16,17].

In this work, we report on two-step resonance ionization spectroscopy performed on $^{249–253}$Cf with resolved HFS for the odd-A isotopes. Especially the measurements on ^{253}Cf with a sample containing only about 5×10^7 atoms (21 fg) demonstrate the outstanding sensitivity of the applied technique.

II. EXPERIMENTAL SETUP

A. Origin and preparation of the samples

The californium samples used in this work were obtained from two different sources. One sample was purchased from Eckert & Ziegler Nuclitec GmbH as 0.1 M nitric acid solution containing the four long-lived isotopes $^{249–252}$Cf. The isotopic composition at the time of the measurement was about 30% ^{249}Cf ($T_{1/2} = 351$ a [15]), 33% ^{250}Cf ($T_{1/2} = 13.08$ a [18]), 16% ^{251}Cf ($T_{1/2} = 898$ a [16]), and 21% ^{252}Cf ($T_{1/2} = 2.645$ a [19]), calculated from the values provided in the technical data sheet corrected for radioactive decay. An aliquot containing 6×10^{11} atoms of californium ($\approx$250 pg) was taken from the solution and dried on a 25-μm-thick zirconium foil. A smaller fraction of this material was already used for preparatory spectroscopic measurements of the atomic structure of californium [10]. Among $^{249–252}$Cf, the second sample contained the more exotic and relatively short-lived isotope ^{253}Cf ($T_{1/2} = 17.81$ d [16]). Originally, this sample was produced at ORNL in the HFIR in 2019 and delivered to Mainz for spectroscopic studies of einsteinium [12] and fermium. Although a chemical separation was performed at ORNL, the long-lived californium isotopes $^{249–252}$Cf were still present in measurable quantity. In 2021, this sample was irradiated with thermal neutrons in the V4 beam tube of the ILL high-flux reactor in Grenoble. The main goal was to produce ^{255}Es from ^{254}Es. However, the californium isotopes in the sample were also transmuted by neutron-capture and produced a sufficiently large amount of ^{253}Cf for laser spectroscopic studies. Heavier californium isotopes were not produced in a quantity large enough for detection due to the high neutron-induced fission cross section $\sigma(n, \text{fission}) = 1300$ b compared with the neutron capture cross section $\sigma(n, \gamma) = 18$ b in ^{253}Cf [20]. The sample was returned to JGU for separation of individual actinide elements and subsequent laser spectroscopic study. The separation of the californium from the einsteinium was performed at the Department of Chemistry's TRIGA site. The sample was dissolved in 0.1 M nitric acid; the californium isolation was performed using an actinide element separation based on α-hydroxyisobutyric acid (α-HIB) on the cation exchanger Mitsubishi CK10Y at 70 °C with a 0.17 M α-HIB solution at pH 4.8. The eluted fraction was transferred on two zirconium foils and evaporated to dryness. The amount of ^{252}Cf in one sample was determined to be approximately 1×10^{11} atoms by α spectrometry. Based on the measured isotope ratio ^{252}Cf : ^{253}Cf (see Sec. III), we evaluated the amount of ^{253}Cf to around 5×10^7 atoms. Note that this was not detectable by α spectrometry due to the small α-decay branch of about 0.3% [16] and thus the amount of ^{253}Cf was unknown prior to the measurements presented here.

B. Ion source and laser system

The zirconium foils backing the samples were folded for complete encasement and delivered to the Institute of Physics at JGU. The high-resolution laser spectroscopy measurements were conducted at the RISIKO mass separator [21]. The samples were inserted into the atomizer tube, which can be resistively heated to a maximum temperature of about 2000 °C. Already at 800 °C neutral californium atoms start to evaporate inside the atomizer and drift towards the open end of the tube. For high-resolution spectroscopy, the effusing atomic beam is intersected perpendicularly by the spectroscopy laser (first step) at a distance of few millimeters from the atomizer. The ionization laser beam (second step) is collinearly overlapped to the atomic beam, therefore further decreasing the effective opening angle within the interaction region. In this way a Doppler width in the order of 50 MHz can be achieved in the first excitation step. The entire laser interaction process takes place within the perpendicularly illuminated laser ion source and trap (PI-LIST), which is described in detail in Ref. [23]. The efficiency loss factor of PI-LIST operation compared with the standard in-source approach typically ranges from 100 to 300 [23], with overall efficiencies estimated to be on the order of 10^{-4} [24]. A sketch of the setup used for high-resolution spectroscopy is depicted in Fig. 1.

The separation of atomization and ionization volume using the PI-LIST enables the suppression of surface-ionized species and electrons from the hot atomizer by two aperture

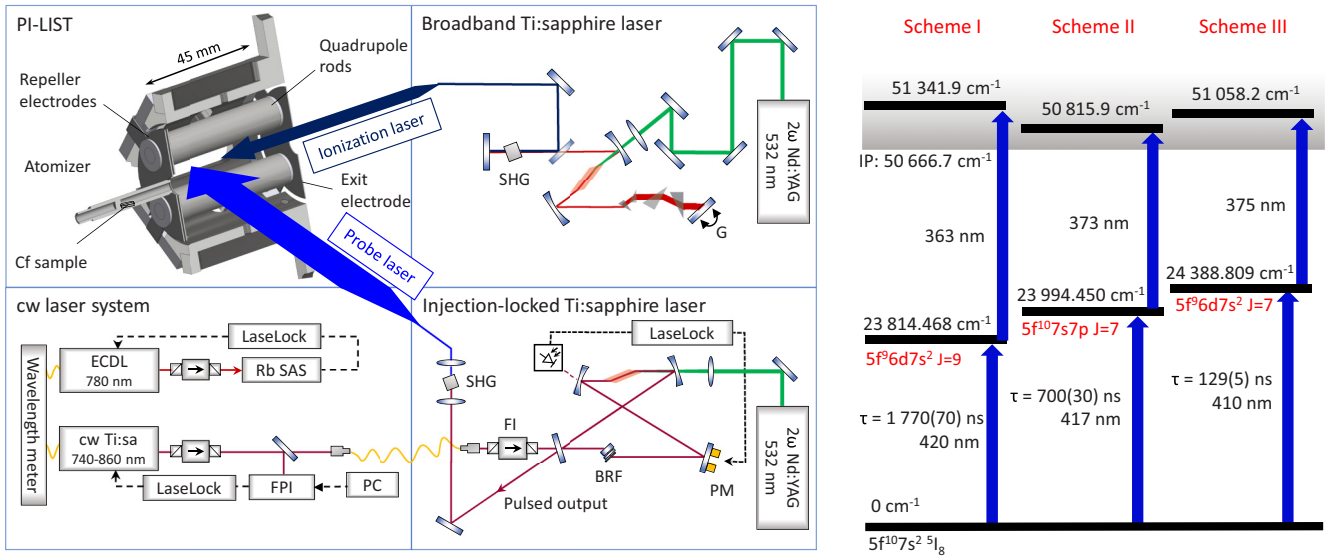

FIG. 1. (left) Sketch of a part of the experimental setup as applied for high-resolution spectroscopy of californium. Abbreviations are used as follows: SHG = second harmonic generation, G = reflective diffraction grating, ECDL = external cavity diode laser, Rb SAS = rubidium saturated absorption spectroscopy, FPI = Fabry-Perot interferometer, FI = Faraday isolator, BRF = birefringent filter, and PM = piezo-mounted mirror. (right) Ionization schemes applied to study the HFS of californium in the first excitation step (FES). The given energy levels refer to ^{250}Cf with an absolute uncertainty of 0.002 cm^{-1} in the FES. The ionization ladders and lifetimes τ are taken from Ref. [10]. Note that in the measurements here not necessarily the strongest autoionizing states were used, but those which provide similar ionization for all hyperfine levels. Figure adapted from Ref. [22].

electrodes. Ions are axially centered by a quadrupolar rf-field, guided to the exit electrode of the LIST by field penetration and are then accelerated to 30 keV. Subsequently, the ions are separated by a 60°-sector-field dipole magnet according to their mass-to-charge ratio, whereby neighboring masses are cutoff by a separator slit in the focal plane of the magnet with a mass resolving power of $M/\Delta M \approx 600$. Finally, the ions are counted by a secondary electron multiplier. Additional background suppression was achieved by time-resolved acquisition of the produced ions with a multichannel analyzer, and gating to the 20- to 30-μs-long ion bunch structure imprinted by the pulsed laser system. This was in particular necessary for the measurements on ^{253}Cf.

In this work, three different resonant two-step ionization schemes were investigated, in the following named schemes I, II, and III, as given in Fig. 1. Thereby, a distinction has to be made between the ionization laser (second step) and the narrowband probe laser for the first excitation step (FES) to an intermediate state. The former is a custom-built grating tuned, z-shaped Ti:sapphire laser featuring intracavity second-harmonic generation (SHG) with an output power of up to 1 W in the region from 360 to 370 nm. The spectral bandwidth is typically on the order of 5 to 7 GHz, and the laser pulse length is in the range of 35–55 ns. The Ti:sapphire laser was pumped with 16 W by a 10 kHz high-repetition rate Nd:YAG laser operating in frequency-doubled mode at 532 nm. The more critical part of the setup is the generation of narrowband laser light applicable to scan across the ground-state transitions. For this purpose, an injection-locked Ti:sapphire laser with a bandwidth on the order of 20 MHz was used [25]. A custom-built direct diode pumped continuous-wave (cw) Ti:sapphire laser acted as a seed laser for injection locking. A detailed description of the laser design and stabilization procedure is provided in Refs. [26,27].

A beta barium borate crystal was used for single-pass SHG of the laser light from the pulsed injection-locked laser resulting in an output power of typically 100 mW for spectroscopy. Finally, the laser beam was horizontally enlarged to about 2 cm in front of the PI-LIST to increase the ionization volume and thus affect the efficiency positively. During the experiment, the fundamental wavelengths of the cw laser and the ionization laser were measured with a High-Finesse WSU-30 wavelength meter with a nominal absolute accuracy of 30 MHz (3σ criterion). This was regularly calibrated to a precisely known rubidium transition during the measurements as described in Ref. [28]. A rather similar setup, except for the new cw-Ti:sapphire laser for seeding, was already used for high-resolution spectroscopy in promethium and technetium [22,24].

III. HIGH-RESOLUTION SPECTROSCOPY

The HFS of the odd-A isotopes ^{249,251,253}Cf and the isotope shifts of the isotopic chain of $^{249-253}$Cf were measured in all three ionization schemes (see Fig. 1). Since the total angular momentum J of all investigated atomic states is larger than the nuclear spin I, each atomic state splits into $2I+1$ HFS levels. According to selection rules, this leads to a total of 27 possible dipole-allowed transitions between the ground and the excited state in ^{249}Cf for all three schemes. To minimize saturation broadening of the transitions, the laser power in the FES was lowered to 1 to 2 mW in all schemes (except

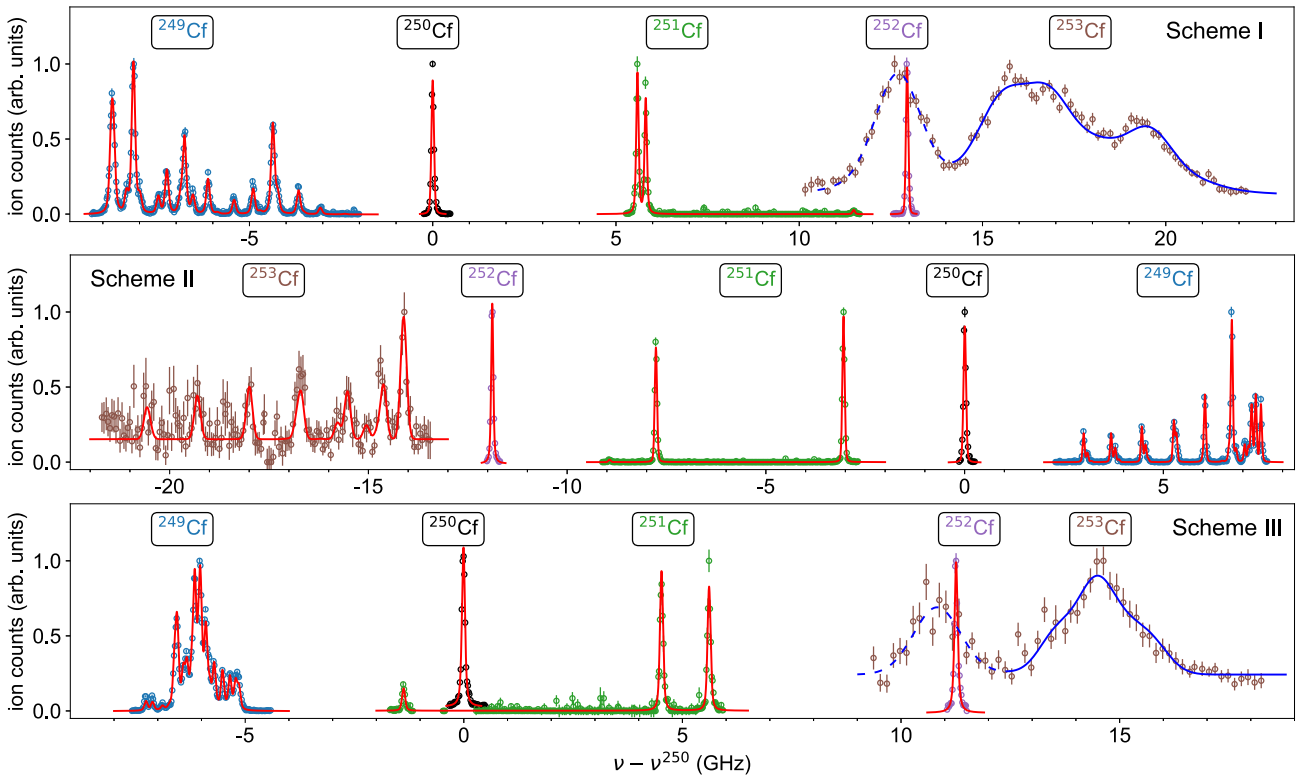

FIG. 2. Measured transitions for $^{249-252}$Cf. In the PI-LIST arrangement resolutions between 50 and 100 MHz were achieved for $^{249-252}$Cf in all three ionization schemes, while ^{253}Cf was included in PI-LIST measurements only for scheme II with a resolution of 180 MHz. The spectra for ^{253}Cf for scheme I and III were measured in-source with resolutions of about 1.5 GHz, whereby the resonance of ^{252}Cf is also included as a reference. The ^{252}Cf part of the spectra is indicated by blue dashed lines. The in-source measurements exhibit a Doppler shift in the order of 100 to 400 MHz to lower transition frequencies compared with the PI-LIST measurements. The red lines represent fits to the data. The blue lines for ^{253}Cf for schemes I and III give fits with respect to the centroid, while the HFS parameters are fixed to the results obtained from the ^{253}Cf fit in scheme II and using the $\mathcal{A}$ and $\mathcal{B}$ ratios determined for ^{251}Cf and ^{249}Cf, respectively.

for measurements on ^{253}Cf, where saturation broadening was accepted and the full laser power of about 100 mW was used to produce a sufficiently intense signal). Additionally, the long half-lives of the excited states allowed for decoupling the ionization process from the excitation, which can deteriorate the spectral resolution and cause slight lineshape distortions from AC Stark shifts [29,30]. For this purpose, the ionization laser pulse was delayed by 150 ns for schemes I and II and by 100 ns for scheme III compared with the FES laser pulse. This was again omitted for measurements on ^{253}Cf. In this way, linewidths down to 55 MHz were achieved for $^{249-252}$Cf under optimum conditions, whereas the linewidth obtained for ^{253}Cf was 180 MHz. The power in the second step was limited to values around 400 to 600 mW, as higher powers strongly influenced the ion signal by additional heating of the sample. The obtained spectra are shown in Fig. 2.

In case of ^{253}Cf, the total amount of atoms was so small that initially only in-source measurements were performed. For these, the PI-LIST structure was removed to increase the overall efficiency of the setup. In this case, the injection-locked laser was illuminating the atomizer collinearly, which led to a Doppler-limited linewidth of typically 1 GHz. A similar approach was performed recently for spectroscopy on einsteinium isotopes [12]. The collinear and perpendicular measurements can be compared because the single resonance of ^{252}Cf was also measured for all frequency scans on ^{253}Cf. This is due to the limited mass resolution, which leads to a leakage of the strong signal on mass 252 to 253. The in-source measurements exhibit a Doppler-shift in the order of 100 to 400 MHz to the PI-LIST measurements due to the movement of the effusing atoms. This was taken into account for an accurate determination of energy levels and isotope shifts. The counting rate on mass 253 was in a range between 1 and 3 counts per second (cps) on the strongest hyperfine components, with a background rate between 0.5 and 1 cps. Correspondingly, a measurement of weaker hyperfine transitions was not possible. The background rate was particularly high on mass 253 and additional heating of the atomizer increased the background faster than the signal. This led to limited statistics of the recorded spectra and hampered a conclusive analysis of the HFS of ^{253}Cf. The ratio ^{252}Cf : ^{253}Cf was determined to about 2000 to 1 by analyzing the heights of the ion signals.

The hyperfine spectra were fit using the SATLAS python package [31]. Although the ratios for the hyperfine parameters of the upper and lower atomic states $\mathcal{A}_l/\mathcal{A}_u$ and $\mathcal{B}_l/\mathcal{B}_u$

TABLE I. Extracted energy positions of atomic levels ^{250}Cf and HFS parameters for the odd-A californium isotopes. The uncertainties were determined by adding a triangle function with arbitrary phase to the measured data to account for possible systematic uncertainties in the wavelength measurement [28]. Note that the ground-state parameters of ^{249}Cf and ^{251}Cf were measured for three transitions and the respective results were averaged. The determined HFS width σ_{expt} for ^{249}Cf is compared with previously reported values σ_{lit} from Ref. [14]. Uncertainties resulting from measurements are given in parentheses, whereas propagated uncertainties due to fixed $\mathcal{A}$ and $\mathcal{B}$ ratios are represented by curly brackets. For more details, see text.

	^{250}Cf	^{249}Cf				^{251}Cf	^{253}Cf	
J	E_{expt} (cm^{-1})	$\mathcal{A}_{\text{expt}}$ (MHz)	$\mathcal{B}_{\text{expt}}$ (MHz)	σ_{expt} (cm^{-1})	σ_{lit} (cm^{-1})	$\mathcal{A}_{\text{expt}}$ (MHz)	$\mathcal{A}_{\text{expt}}$ (MHz)	$\mathcal{B}_{\text{expt}}$ (MHz)
8	0	−53.4(2)	2991(10)	0.15	0 (fixed)	−693.7(11)	−127(3)	2640(200)
9	23 814.468(2)	−46.1(3)	12 570(20)	0.30		−597(2)	−109{3}[a]	11 100{850}[a]
7	23 994.450(2)	−12.3(3)	−1285(15)	0.035	0.14	−156(2)	−28.6{7}[b]	−1130{90}[b]
7	24 388.809(2)	−70.7(7)	3875(40)	0.18	0.01	−930.9(14)	−170{4}[a]	3430{260}[a]

[a]HFS parameters calculated from the ground state values using the ratios obtained for ^{251}Cf and ^{249}Cf, respectively.
[b]The ratio of this level to the ground state was fixed in the fitting procedure to the ratio known from ^{251}Cf and ^{249}Cf, respectively.

were precisely known from the spectra of ^{251}Cf and ^{249}Cf, respectively, and fixed during the fitting process; a conclusive fit for ^{253}Cf was not possible from the in-source scans due to the low resolution and the 21 underlying hyperfine transitions. Therefore, the second sample containing ^{253}Cf was used to perform spectroscopy in the PI-LIST. Despite the lower efficiency, it was possible to record one spectrum for scheme II while exhausting the complete sample. This was only possible due to the enhanced background suppression in PI-LIST operation. Note that the statistics on the left side of this ^{253}Cf spectrum deteriorated during the scan, as the sample was depleting and the background slowly increased gradually during heating.

Table I summarizes the obtained HFS parameters for the odd-A isotopes for different atomic energy levels. For ^{253}Cf, the measured spectrum in scheme II with high resolution can be matched by a fit only for an assignment of $I = 7/2$, which confirms the tentatively allocated value of the nuclear spin. For the ground state in ^{249}Cf, $\mathcal{A}_l = -53.4(2)$ MHz and $\mathcal{B}_l = 2991(10)$ MHz result as the weighted mean of the three measured transitions. This gives a total HFS splitting of 4.5 GHz (0.15 cm^{-1}). In their analysis of spectra obtained from electrodeless lamps, Conway *et al.* assumed the width of the ground state splitting in ^{249}Cf to be small and set it as zero for their analysis based on observations in americium [14]. Following this assumption, they determined ^{249}Cf HFS widths for many other states, such as that at 23 994 cm^{-1} to a value of 0.14 cm^{-1} and at 24 388.60 cm^{-1} to 0.01 cm^{-1}, respectively, as given in Table I. As our results show, this assumption is clearly not valid. Therefore, the HFS widths reported by Conway *et al.* refer to the observed transition width, while the HFS information for the respective levels has to be corrected accordingly. Table I compares the accurately determined values in this work with those of Conway *et al.* [14].

A. Isotope shifts

The rather large size of the isotope shift, in the order of 5 GHz, is clearly visible in Fig. 2. It is defined as the center frequency shift in an optical transition i between two isotopes with mass numbers A and A':

$$\delta\nu_i^{AA'} = \nu_i^{A'} - \nu_i^{A}. \tag{1}$$

The shift is caused by the different masses of the isotopes in the form of a normal and a specific mass effect as well as by the change in the mean-squared charge radius of the nucleus, $\delta\langle r_c^2\rangle^{AA'}$. The latter contributes in conjunction with an atomic-transition-dependent field shift constant F_i. In this way the isotope shift can be expressed as

$$\delta\nu_i^{AA'} = \frac{K_{i,\text{NMS}} + K_{i,\text{SMS}}}{\mu} + F_i\delta\langle r_c^2\rangle^{AA'}, \tag{2}$$

with the mass-scaling factor $\mu = m_{A'}m_A/(m_{A'} - m_A)$. While the constant for the normal mass shift (NMS) can be calculated by $K_{i,\text{NMS}} = m_e\nu$ with m_e being the mass of the electron, the constant for the specific mass shift (SMS) can only be estimated. Here it is assumed to be $K_{i,\text{SMS}} = 0 \pm K_{i,\text{NMS}}$ for scheme II because $K_{i,\text{SMS}}$ is typically smaller than $K_{i,\text{NMS}}$ for $s-p$ transitions [32]. However, for transitions involving f or d electrons (schemes I and III), $K_{i,\text{SMS}}$ can be ten or more times larger [32]. In any case, the contribution of the mass shift is orders of magnitudes smaller than the field shift in the range of heavy elements like californium [1]. In our case, the NMS is on the order of just 0.1% of the total isotope shift and therefore mass shift corrections can be omitted. Table II summarizes the measured isotope shifts with respect to ^{250}Cf, i.e., the isotope exhibiting the $N = 152$ shell closure. The sign of the isotope shift contains information about the electronic configuration of the involved atomic levels. It is expected that the transition

TABLE II. Measured isotope shifts for three transitions compared with the reference isotope ^{250}Cf in MHz.

Isotope	$>\delta\nu_{420}^{250,A'}$	$\delta\nu_{417}^{250,A'}$	$\delta\nu_{410}^{250,A'}$
^{249}Cf	−6812(12)	6250(12)	−5921(12)
^{250}Cf	0	0	0
^{251}Cf	5721(14)	−5274(12)	5013(12)
^{252}Cf	12 944(14)	−11 887(14)	11 265(14)
^{253}Cf	17 470(50)	−16 052(20)	15 230(75)

energy is larger for lighter isotopes for transitions from a lower s state to a higher p state. From the configurations given in Fig. 1 this is expected for the line at 417 nm, which agrees with our measurement. The other two are transitions with an electron being excited from a f orbital into an d orbital, where an opposite sign of the isotope shift is expected, which is also confirmed by our results. The determination of changes in the mean-squared charge radii is of particular interest. At present, no experimental data on charge radii in californium or atomic calculations for the field shift parameter F for any transition are available. An analysis of the absolute changes in charge radii is therefore not possible, but variations in the isotope shift data, which linearly translate to irregularities in the evolution of mean-squared charge radii, can be assessed. Although only one isotope below $N = 152$ is included in our measurements, the isotope shift values do not explicitly reveal a pronounced kink at $N = 152$, as it is the case in chains of other elements at the $N = 126$ or $N = 82$ shell closures. More definite statements would require further measurements on additional more neutron-deficient isotopes.

A normal odd-even staggering becomes apparent, which can be quantified by the staggering parameter

$$\gamma_A = \frac{\delta\langle r_c^2\rangle^{A-1,A}}{\delta\langle r_c^2\rangle^{A-1,A+1}} = \frac{2\delta\nu_{i,F}^{A-1,A}}{\delta\nu_{i,F}^{A-1,A+1}}, \tag{3}$$

without any knowledge of the F factor or of charge radii [33]. Note that Eq. (3) is typically defined for odd neutron numbers. In this case, the isotope shifts for respective neighboring isotopes have to be known. However, since we measured three odd-A isotopes and two even-A isotopes, it is calculated here for even neutron numbers. This means normal odd-even staggering is represented by $\gamma_A > 1$. The results obtained for scheme II are used to determine the staggering parameter, as the contribution of the mass shift can be estimated best for this scheme and ^{253}Cf could also be measured most precisely in this scheme. This finally yields $\gamma_{250} = 1.086(4)$ and $\gamma_{252} = 1.227(5)$, which shows that the investigated californium isotopes exhibit normal odd-even staggering. The increase for ^{252}Cf indicates that the odd-even staggering becomes more pronounced for larger neutron numbers. For lighter actinides like thorium, uranium, and plutonium, similar staggering parameters, i.e., $\gamma_{228}^{\mathrm{Th}} = 1.09$, $\gamma_{234}^{\mathrm{U}} = 1.31$, and $\gamma_{240}^{\mathrm{Pu}} = 1.36$, were calculated using changes in mean-squared charge radii as given in Ref. [6].

A modified King plot analysis was performed for the data in Table II to verify the reliability of the measured isotope shifts. Equation (2) can be rewritten for two transitions i, j to

$$\mu\delta\nu_i^{AA'} = \frac{F_i}{F_j}\mu\delta\nu_j^{AA'} + \left(M_i - \frac{F_i}{F_j}M_j\right), \tag{4}$$

with $M_{i,j} = K_{i,j,\mathrm{NMS}} + K_{i,j,\mathrm{SMS}}$. In Fig. 3, the modified isotope shift $\mu\delta\nu_{417}^{AA'}$ is plotted against $\mu\delta\nu_{420}^{AA'}$ and $\mu\delta\nu_{410}^{AA'}$, respectively. The data points should follow a linear trend with a slope of $\frac{F_i}{F_j}$ and a y intercept of $M_i - \frac{F_i}{F_j}M_j$. Due to the lack of information on F, the absolute slope values cannot be checked. Nevertheless, the observed linearity is a direct test for the consistency of the measured data. For the linear regression, uncertainties in both variables were taken into account. The fit results are given in Table III. In both cases, the y intercept is relatively small (compared with the x- and y-axis values in Fig. 3) and includes zero within its uncertainty. This is in good agreement with the assumption of a small mass shift, as $K_{\mathrm{NMS}} \approx 0.4$ THz u and the SMS is assumed to be in the same order of magnitude. The χ^2_{red} value is smaller than one, suggesting that the uncertainties in the isotope shifts might be somewhat overestimated.

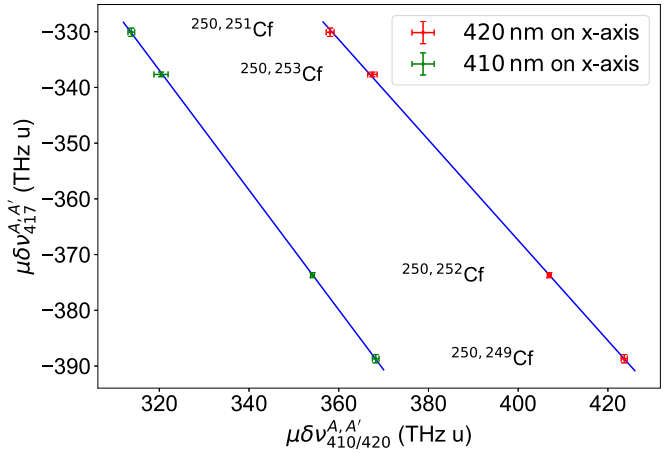

FIG. 3. Modified King plot on the measured ground-state transitions in californium. The modified isotope shift for the transition at 417 nm (y axis) is drawn against the modified isotope shift for the transitions at 410 nm (green data points) and 420 nm (red data points) on the x axis. The blue lines represent linear fits to the data points.

B. Nuclear moments

The HFS parameters $\mathcal{A}$ and $\mathcal{B}$ are given in Table I. They are directly linked to the magnetic moment μ_I and the spectroscopic electric-quadrupole moment Q_S of the nucleus by the relations

$$\mathcal{A} = \mu_I \frac{B_e(0)}{IJ} \quad \text{and} \quad \mathcal{B} = eQ_S\left\langle\frac{\partial^2 V}{\partial z^2}\right\rangle_{z=0}. \tag{5}$$

A determination of the nuclear moments requires knowledge of the magnetic field at the location of the nucleus $B_e(0)$ and of the electric-field gradient inside the nucleus $\langle\partial^2 V/\partial z^2\rangle_{z=0}$. These values can either be determined by comparison to the hyperfine parameters of other, often stable, isotopes, for which the moments are known from complementary measurement techniques, or they can be estimated from accurate atomic theory calculations [1,2]. For

TABLE III. Ratios of the field shifts constants for two pairs of transitions are extracted from the King-plot, corresponding to the slope of the fit in Fig. 3. Additionally, the y-axis intercept is listed in the third column, which gives hints at the contribution of the mass shift.

i, j	$\frac{F_i}{F_j}$	$M_i - \frac{F_i}{F_j}M_j$ (THz u)	χ^2_{red}
417, 420	−0.901(18)	−7.2(71)	0.19
417, 410	−1.075(25)	7.1(86)	0.03

TABLE IV. Magnetic dipole ($\mathcal{A}$) and electric quadrupole ($\mathcal{B}$) HFS constants of the ground state of dysprosium and californium with experimental values for dysprosium taken from Ref. [34]. Nuclear parameters $\mu_I = -0.480(3)\mu_N$, $I = 5/2$, $Q_S = 2.51(2)$ eb were used for ^{161}Dy and $\mu_I = 0.673(4)\mu_N$, $I = 5/2$, $Q_S = 2.65(2)$ eb were used for ^{163}Dy [35,36]. Theoretical uncertainties for californium are inferred from the difference between theory and experiment for dysprosium.

		Calculations		Experiment	
Atom	State	$\mathcal{A}$ (MHz)	$\mathcal{B}$ (MHz)	$\mathcal{A}$ (MHz)	$\mathcal{B}$ (MHz)
^{161}Dy	$4f^{10}6s^2\ ^5I_8$	−113	1127	−116.231(2)	1091.577(50)
^{163}Dy	$4f^{10}6s^2\ ^5I_8$	158	1190	162.754(2)	1152.869(40)
Dy	$4f^{10}6s^2\ ^5I_8$	$587(\mu_I/I)$	$449Q_S$	$605(3)(\mu_I/I)$	$435(3)Q_S$
Cf	$5f^{10}7s^2\ ^5I_8$	$608(18)(\mu_I/I)$	$477(16)Q_S$		

californium, only the magnetic moment of ^{249}Cf was determined to $\mu_I(^{249}\text{Cf}) = -0.28(6)\mu_N$. The sign was deduced from optical spectroscopy [14] and the absolute value from electron paramagnetic resonance measurements on Cf^{3+} carried out in 1975 in conjunction with atomic calculations. The latter are the dominating contribution to the uncertainty [13]. Due to recent improvements in atomic theory and related codes, new atomic calculations were performed for dysprosium and californium within this work. Dysprosium is the homologue atomic system for which the HFS is experimentally known. It has an electronic structure analog to that of californium.

Comparing theoretical atomic calculations and experimental data for dysprosium enables an evaluation of the achievable accuracy. The atomic coupling constants are obtained using the configuration interaction with perturbation theory method (CIPT) [37]. Both atomic systems are treated as atoms with twelve external electrons in open shells, $4f^{10}6s^2$ for Dy and $5f^{10}7s^2$ for Cf. The V^{N-1} approximation is used to generate the basis. The method of random-phase approximation (RPA) is used to build the effective HFS operator (see, e.g., Ref. [38]). The HFS of the many-electron state a is given by

$$\delta E_a = \langle a| \sum_i \hat{H}_i^{\text{HFS}} + \delta V_i^{N-1} |a\rangle. \tag{6}$$

Here summation goes over twelve external electrons, and δV_i^{N-1} is the atomic core polarization correction to the HFS operator $\hat{H}_i^{\text{HFS}}$. The results are summarized in Table IV and show agreement of the calculated values with the experimental data within about 3% in dysprosium. An additional uncertainty can be expected for californium from details in the nuclear charge distribution as well as from nuclear polarization effects, which are summarized under the term hyperfine anomaly and estimated to 1%–2%. This is supported by the experimental observation that all ratios of spin-normalized HFS constants $\mathcal{A}$ from the different investigated transitions agree within their uncertainty to 2%, with no obvious sign of hyperfine anomaly, even though changes in the electron configuration from s to p orbitals as well as from f to d orbitals are addressed.

With the new theoretical calculations and the weighted mean values for the ground state HFS parameters, as given in Table I, the magnetic moments and spectroscopic quadrupole moments can be determined with a precision added on the order of 5% to 10% as summarized in Table V. The newly determined magnetic moment of $\mu_I(^{249}\text{Cf}) = -0.395(17)\mu_N$ changes the literature value by about 2σ and is ≈5 times more precise. In addition, the previously unknown magnetic-dipole moments of $\mu_I(^{251}\text{Cf}) = -0.571(24)\ \mu_N$ and $\mu_I(^{253}\text{Cf}) = -0.731(35)\ \mu_N$ are extracted.

The magnetic-dipole moment probes the single-particle properties of the unpaired neutron for the odd-A californium isotopes. Therefore, our experimental values are compared with nuclear theory calculations by the Hartree-Fock-Bogolyubov (HFB) formalism, which is well known to provide a reliable description of the nuclear ground-state properties of even-even systems. This also serves as a starting point to improve the description of ground-state properties for systems with an odd numbers of nucleons [39]. At the static mean-field level, the solutions of the HFB equations are quasiparticle (qp) orbitals, which set a so-called "vacuum" corresponding to a $J^\pi = 0^+$ state. The HFB ground state of even-even nuclei is determined by minimizing the binding energy over the entire potential-energy surface (PES) in the deformation plane. To describe fermion systems, such as nuclei with an odd number of nucleons, the ground state should be redefined as the excitation of one qp state on top of a HFB vacuum. In practice, the qp excitation that minimizes the total energy is selected. In the present axially symmetric HFB framework, the projection K of the total angular momentum J and the parity π are good quantum numbers. Thus, the HFB ground state for odd-A nuclei with spin-parity J^π is described by selecting a qp orbital with $K_{qp}^\pi = J^\pi$ and imposing its occupation probability. This so-called blocking approximation can be limited to the equal filling one, where time-reversal symmetry is conserved. After variation, only one of the two qp

TABLE V. Extracted nuclear moments for ^{249}Cf, ^{251}Cf, and ^{253}Cf using experimental values in combination with the CIPT atomic calculations. In addition, the magnetic-dipole moments $\mu_{I,\text{HFB}}$ and spectroscopic quadrupole moments $Q_{S,\text{HFB}}$ obtained by nuclear HFB calculations are given.

Isotope	I	μ_I (μ_N)	$\mu_{I,\text{HFB}}$ (μ_N)	Q_S (eb)	$Q_{S,\text{HFB}}$ (eb)
^{249}Cf	9/2	−0.395(17)[a]	−0.731	6.27(33)	6.86
^{251}Cf	1/2	−0.571(24)	−1.015		
^{253}Cf	7/2	−0.731(35)	−0.755	5.53(51)	5.40

[a] $\mu_{I,\text{Lit}} = -0.28(6)\mu_N$ from Ref. [13].

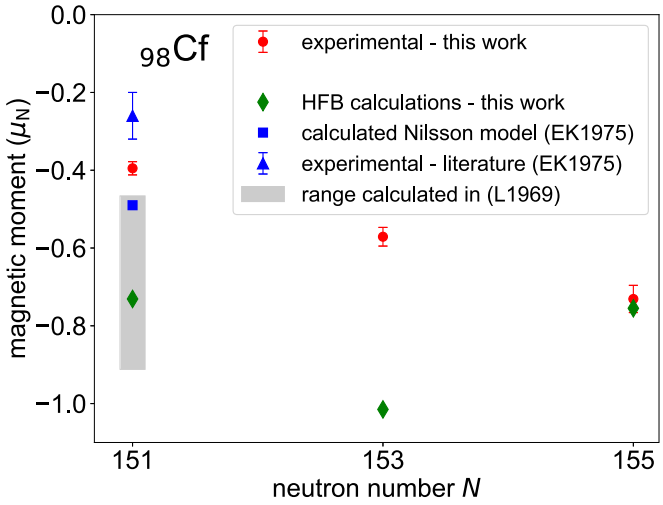

FIG. 4. Comparison of experimental and calculated magnetic-dipole moments in californium (EK1975: [13]; L1969: [43]). The experimental values determined in this work are given in red.

of the blocked pair is considered as an excitation on top of the HFB vacuum to calculate observables within time breaking assessment.

In the current study, HFB calculations have been performed for californium isotopes starting from ^{248}Cf up to ^{254}Cf with 16 harmonic-oscillator major shells using the D1M interaction [40]. For odd-A californium isotopes, all possible blockings are considered including not only the first blocked qp for a given K^π but also the second (and up to the third if $K = 1/2$ or $3/2$). Indeed, as shown in Ref. [39], we are not certain that blocking the orbital, which yields the lowest ground-state energy, corresponds to the observed nuclear spin neither to the magnetic moment. As far as the ground state spins are concerned, it turns out that our predictions agree with the experiment for ^{249}Cf and ^{251}Cf. However, for ^{253}Cf two near-degenerate states are predicted within 4 keV: one with spin projection and parity $K^\pi = 1/2^+$, and another with $K^\pi = 7/2^+$, which corresponds to the experimentally observed ground state. For each blocked qp, a PES is computed as function of the quadrupole deformation and all relevant observables (magnetic moment, isotopic shift, and spectroscopic quadrupole moment) are deduced both for the minimum of the PES and, to take possible configuration mixing into account, by averaging over deformation, as described in Ref. [41]. However, due to the rigidity of the PES for all the californium isotopes [42], this average does not have much impact on the results, in contrast to what was found in Ref. [41]. The magnetic-dipole moments of the isotopes ^{249,251,253}Cf are compiled graphically in Fig. 4 together with the theoretical predictions.

For ^{249}Cf, the newly determined experimental value for the nuclear magnetic dipole moment of $\mu_I(^{249}\mathrm{Cf}) = -0.395(17)\mu_\mathrm{N}$ agrees reasonably well with the absolute value of the reported magnetic moment $|\mu_I(^{247}\mathrm{Cm})| = 0.36\mu_\mathrm{N}$ for the same $9/2^-[734]$ neutron orbital in ^{247}Cm [44]. In addition, the new experimental value is closer to the estimated moment of $\mu_{9/2^-[734]} = -0.49\mu_\mathrm{N}$ obtained by using effective g factors for the $9/2^-[734]$ Nilsson configuration by Edelstein *et al.* who determined the magnetic moment for the first time [13]. A similar value of $\mu_I(^{249}\mathrm{Cf}) = -0.466\mu_\mathrm{N}$ was calculated in Ref. [43] assuming the spin g_s factor of the unpaired neutron to be $g_s = 0.6g_s^{\mathrm{free}}$, while for $g_s = g_s^{\mathrm{free}}$ a magnetic moment of $\mu_I(^{249}\mathrm{Cf}) = -0.912\mu_\mathrm{N}$ is reported. The HFB calculations result in a magnetic-dipole moment of $\mu_I(^{249}\mathrm{Cf}) = -0.731\mu_\mathrm{N}$ which has the correct sign and lies well in the range of the aforementioned values from effective model estimates, but is significantly larger than the experimental value. This is similar for ^{251}Cf, for which μ_I is overestimated by a similar factor with comparison to the experiment, while the HFB calculation agrees perfectly with the experimental value for ^{253}Cf, as visualized in Fig. 4. From the fact that all magnetic moments in general exhibit a negative sign, we can deduce that a parallel pairing of spin and orbital momentum is preferred. Apart of that, the single-particle character of the unpaired neutron seems to be significantly reduced close to $N = 152$, either by configuration mixing or by an imperfect momentum coupling, which is not completely reproduced by the HFB calculations.

In addition to the nuclear magnetic-dipole moments, also the spectroscopic electric-quadrupole moments Q_S of the nuclei can be deduced from the hyperfine parameter $\mathcal{B}$ using the atomic CIPT calculations at a similar level of uncertainty. The deduced Q_S values for ^{249}Cf and ^{253}Cf are given in Table V. From the spectroscopic quadrupole moments Q_S, the intrinsic quadrupole deformation Q_0 can be calculated using

$$Q_0 = \frac{(I+1)(2I+3)}{3K^2 - I(I+1)} Q_\mathrm{S}, \tag{7}$$

assuming $K = I$ for the nuclear ground state and well-deformed nuclei [45]. This results in $Q_0(^{249}\mathrm{Cf}) = 11.5(6)\ e\mathrm{b}$ and $Q_0(^{253}\mathrm{Cf}) = 11.8(11)\ e\mathrm{b}$, indicating a stable quadrupole deformation across $N = 152$. This is in line with the trend observed for ^{253,254,255}Es [12], albeit the deformation in the einsteinium isotopes is slightly larger. The deformation parameter $\beta \approx 0.27$ deduced for both californium isotopes, obtained using the relation $Q_0 = \frac{3}{\sqrt{5\pi}} ZeR_0^2\beta$, valid for nuclei with one symmetry axis and the nuclear radius of $R_0 = 1.2A^{1/3}$, agrees very well with the deformation of $\beta(^{249}\mathrm{Cf}) \approx 0.28$ and $\beta(^{253}\mathrm{Cf}) \approx 0.27$ obtained in the HFB calculations. The good agreement is also evident by comparing the calculated spectroscopic quadrupole moments $Q_{\mathrm{S,HFB}}$ with the experimentally determined values Q_S in Table V.

IV. SUMMARY

High-resolution laser spectroscopy was performed on the isotopes $^{249-253}$Cf across the deformed $N = 152$ neutron shell closure at ^{250}Cf and using samples sizes down to the fg scale in the case of ^{253}Cf. Three different optical transitions were investigated spectroscopically and isotope shifts as well as hyperfine parameters were extracted. Even though the field shift constants for californium are not known, which hampers the extraction of changes in the mean-squared charge radii, the isotope shifts were analyzed in a relative manner, independent of the absolute changes of the radii. This is reasonable because the mass shift contributes only weakly for heavy nuclei. No hints of shape variations or distortions at the shell closure were found in the investigated small range around the shell gap.

Analyzing the staggering parameter reveals a weak normal odd-even staggering that increases for larger N. The quality and consistency of the isotope shift data was confirmed by a King-plot analysis. Based on these results, on-line measurements of short-lived neutron-deficient californium isotopes, produced in fusion evaporation reactions, are foreseen to study a wider range of nuclei, mapping the behavior in the region of well-deformed heavy nuclei. The hyperfine structure parameters $\mathcal{A}$ and $\mathcal{B}$ were extracted with high precision. A significant inconsistency to the previous assumption of a nearly vanishing ground state splitting was observed in the case of ^{249}Cf. The experimental results of the ground state hyperfine parameters were combined with CIPT atomic calculations, which are now able to access electronic systems with open f shells. The obtained atomic coupling constants enabled an independent determination of the nuclear magnetic-dipole and spectroscopic electric-quadrupole moments for the studied odd-A isotopes. The relative precision for the magnetic-dipole moment of ^{249}Cf was improved by a factor of five and a deviation compared with the literature value was found. These values are compared with nuclear HFB calculations, which show a very good agreement for ^{253}Cf. The calculated nuclear dipole moments for the nuclei directly around $N = 152$ are larger than the experimental data, pointing to an influence on the single-particle behavior at the $N = 152$ shell closure, for which the presented results provide a new point of view.

ACKNOWLEDGMENTS

This research was supported by the U.S. Department of Energy, Office of Science, Office of Basic Energy Sciences, Heavy Elements Chemistry Program, under Award No. DE-FG02-13ER16414. The ^{253}Cf isotope used in this research was supplied by ILL Grenoble], with pre-products delivered by the U.S. DOE Isotope Program, managed by the Office of Science. This work has been supported by the Bundesministerium für Bildung und Forschung (BMBF, Germany) under Grant No. 05P18UMCIA. This project has received funding from the European Union's Horizon 2020 research and innovation program under Grant Agreement No. No. 861198-LISA-H2020-MSCA-ITN-2019. The work of V.A.D. and V.V.F. was supported by the Australian Research Council Grants No. DP190100974 and No. DP200100150. This work has been supported by the Japan Science and Technology Agency (JST) PRESTO Grant No. JPMJPR19G7 and JST SCORE University Promotion Type (Developing the Environment for Creation of Startup Ecosystem in Startup Cities Type), Grant No. JPMJST2076.

[1] P. Campbell, I. D. Moore, and M. R. Pearson, Prog. Part. Nucl. Phys. **86**, 127 (2016).
[2] X. F. Yang, S. J. Wang, S. G. Wilkins, and R. F. Garcia Ruiz, Prog. Part. Nucl. Phys **129**, 104005 (2023).
[3] S. A. Giuliani, Z. Matheson, W. Nazarewicz, E. Olsen, P.-G. Reinhard, J. Sadhukhan, B. Schuetrumpf, N. Schunck, and P. Schwerdtfeger, Rev. Mod. Phys. **91**, 011001 (2019).
[4] A. Ghiorso, S. G. Thompson, G. H. Higgins, B. G. Harvey, and G. T. Seaborg, Phys. Rev. **95**, 293 (1954).
[5] E. M. Ramirez, D. Ackermann, K. Blaum, M. Block, C. Droese, C. E. Düllmann, M. Dworschak, M. Eibach, S. Eliseev, E. Haettner, F. Herfurth, F. P. Heßberger, S. Hofmann, J. Ketelaer, G. Marx, M. Mazzocco, D. Nesterenko, Y. N. Novikov, W. R. Plaß, D. Rodríguez, C. Scheidenberger, L. Schweikhard, P. G. Thirolf *et al.*, Science **337**, 1207 (2012).
[6] I. Angeli and K. P. Marinova, At. Data Nucl. Data Tables **99**, 69 (2013).
[7] M. Block, M. Laatiaoui, and S. Raeder, Prog. Part. Nucl. Phys. **116**, 103834 (2021).
[8] H.-J. Kluge and W. Nörtershäuser, Spectrochim. Acta, Part B **58**, 1031 (2003)
[9] S. M. Robinson, D. E. Benker, E. D. Collins, J. G. Ezold, J. R. Garrison, and S. L. Hogle, Radiochim. Acta **108**, 737 (2020).
[10] F. Weber, C. E. Düllmann, V. Gadelshin, N. Kneip, S. Oberstedt, S. Raeder, J. Runke, C. Mokry, P. Thörle-Pospiech, D. Studer, N. Trautmann, and K. Wendt, Atoms **10**, 51 (2022).
[11] F. Weber, T. E. Albrecht-Schönzart, M. Block, P. Chhetri, C. E. Düllmann, J. G. Ezold, V. Gadelshin, A. N. Gaiser, F. Giacoppo, R. Heinke, T. Kieck, N. Kneip, M. Laatiaoui, C. Mokry, S. Nothhelfer, S. Raeder, J. Runke, F. Schneider, J. M. Sperling, D. Studer *et al.* Phys. Rev. Res. **4**, 043053 (2022).
[12] S. Nothhelfer, T. E. Albrecht-Schönzart, M. Block, P. Chhetri, C. E. Düllmann, J. G. Ezold, V. Gadelshin, A. Gaiser, F. Giacoppo, R. Heinke, T. Kieck, N. Kneip, M. Laatiaoui, C. Mokry, S. Raeder, J. Runke, F. Schneider, J. M. Sperling, D. Studer, P. Thörle-Pospiech *et al.* Phys. Rev. C **105**, L021302 (2022).
[13] N. Edelstein and D. G. Karraker, J. Chem. Phys. **62**, 938 (1975).
[14] J. G. Conway, E. F. Worden, and J. Blaise, J. Opt. Soc. Am. B **12**, 1186 (1995).
[15] K. Abusaleem, Nucl. Data Sheets **112**, 2129 (2011).
[16] E. Browne and J. K. Tuli, Nucl. Data Sheets **114**, 1041 (2013).
[17] I. Ahmad and E. Horwitz, Nucl. Phys. A **373**, 434 (1982).
[18] Y. A. Akovali, Nucl. Data Sheets **94**, 131 (2001).
[19] N. Nica, Nucl. Data Sheets **106**, 813 (2005).
[20] B. J. Allen, J. H. Gibbons, and R. L. Macklin, Adv. Nucl. Phys. **4**, 205 (1971).
[21] T. Kieck, S. Biebricher, C. E. Düllmann, and K. Wendt, Rev. Sci. Instrum. **90**, 053304 (2019).
[22] D. Studer, J. Ulrich, S. Braccini, T. S. Carzaniga, R. Dressler, K. Eberhardt, R. Heinke, U. Köster, S. Raeder, and K. Wendt, Eur. Phys. J. A **56**, 69 (2020).
[23] R. Heinke, T. Kron, S. Raeder, T. Reich, P. Schönberg, M. Trümper, C. Weichhold, and K. Wendt, Hyperfine Interact. **238**, 6 (2017).
[24] T. Kron, R. Beerwerth, S. Raeder, S. Fritzsche, R. Heinke, P. Scönberg, M. Trümper, and K. Wendt, Phys. Rev. C **102**, 034307 (2020).
[25] V. Sonnenschein, I. D. Moore, S. Raeder, M. Reponen, H. Tomita, and K. Wendt, Laser Phys. **27**, 085701 (2017).
[26] V. Sonnenschein, H. Tomita, K. Kotaro, H. Koya, D. Studer, R. Terabayashi, F. Weber, K. Wendt, N. Nishizawa, and T. Iguchi, Hyperfine Interact. **241**, 32 (2020).

[27] V. Sonnenschein, M. Ohashi, H. Tomita, and T. Iguchi, Nucl. Instrum. Methods Phys. Res., Sect. B **463**, 512 (2020).
[28] M. Verlinde, K. Dockx, S. Geldhof, K. König, D. Studer, T. E. Cocolios, R. P. de Groote, R. Ferrer, Y. Kudryavtsev, T. Kieck, I. Moore, W. Nörtershäuser, S. Raeder, P. van den Bergh, P. van Duppen, and K. Wendt, Appl. Phys. B: Lasers Opt. **126**, 85 (2020).
[29] R. P. de Groote, M. Verlinde, V. Sonnenschein, K. T. Flanagan, I. Moore, and G. Neyens, Phys. Rev. A **95**, 032502 (2017).
[30] Á. Koszorús, X. F. Yang, J. Billowes, C. L. Binnersley, M. L. Bissell, T. E. Cocolios, G. J. Farooq-Smith, R. P. de Groote, K. T. Flanagan, S. Franchoo, R. F. Garcia Ruiz, S. Geldhof, W. Gins, A. Kanellakopoulos, K. M. Lynch, G. Neyens, H. H. Stroke, A. R. Vernon, K. D. A. Wendt, and S. G. Wilkins, Phys. Rev. C **100**, 034304 (2019).
[31] W. Gins, R. P. de Groote, M. L. Bissell, C. Granados Buitrago, R. Ferrer, K. M. Lynch, G. Neyens, and S. Sels, Comput. Phys. Commun. **222**, 286 (2018).
[32] K. Heilig and A. Steudel, At. Data Nucl. Data Tables **14**, 613 (1974).
[33] A. E. Barzakh, J. G. Cubiss, A. N. Andreyev, M. D. Seliverstov, B. Andel, S. Antalic, P. Ascher, D. Atanasov, D. Beck, J. Bieroń, K. Blaum, C. Borgmann, M. Breitenfeldt, L. Capponi, T. E. Cocolios, T. Day Goodacre, X. Derkx, H. de Witte, J. Elseviers, D. V. Fedorov, V. N. Fedosseev, C. van Beveren, P. van den Bergh, and P. van Duppen, Phys. Rev. C **99**, 054317 (2019).
[34] W. J. Childs, Phys. Rev. A **2**, 1692 (1970).
[35] J. Emsley, *The Elements*, Oxford Chemistry Guides (Oxford University Press, New York, 1995).
[36] N. J. Stone, Atomic Data and Nuclear Data Tables **111–112**, 1 (2016).
[37] V. A. Dzuba, J. C. Berengut, C. Harabati, and V. V. Flambaum, Phys. Rev. A **95**, 012503 (2017).
[38] V. A. Dzuba, V. V. Flambaum, P. G. Silvestrov, and O. P. Sushkov, J. Phys. B: At. Mol. Phys. **20**, 1399 (1987).
[39] S. Péru, S. Hilaire, S. Goriely, and M. Martini, Phys. Rev. C **104**, 024328 (2021).
[40] S. Goriely, S. Hilaire, M. Girod, and S. Péru, Phys. Rev. Lett. **102**, 242501 (2009).
[41] A. Barzakh, A. N. Andreyev, C. Raison, J. G. Cubiss, P. Van Duppen, S. Péru, S. Hilaire, S. Goriely, B. Andel, S. Antalic, M. Al Monthery, J. C. Berengut, J. Bieroń, M. L. Bissell, A. Borschevsky, K. Chrysalidis, T. E. Cocolios, T. Day Goodacre, J. P. Dognon, M. Elantkowska, E. Eliav, J. G. Farooq-Smith, D. V. Fedorov, R. F. Garcia Ruiz, and A. V. Zaitsevskii, Phys. Rev. Lett. **127**, 192501 (2021).
[42] S. Hilaire and M. Girod, Eur. Phys. J. A **33**, 237 (2007).
[43] I. L. Lamm, Nucl. Phys. A **125**, 504 (1969).
[44] M. M. Abraham, L. A. Boatner, C. B. Finch, R. W. Reynolds, and W. P. Unruh, Phys. Lett. A **44**, 527 (1973).
[45] K. Löbner, M. Vetter, and V. Hönig, At. Data Nucl. Data Tables **7**, 495 (1970).